



# Concentrate and degrade PFOA with a photo-regenerable composite of In-doped TNTs@AC

Jan-Max Arana Juve<sup>a</sup>, Fan Li<sup>b,c</sup>, Yangmo Zhu<sup>b</sup>, Wen Liu<sup>c</sup>, Lars D.M. Ottosen<sup>a</sup>, Dongye Zhao<sup>b,\*\*</sup>, Zongsu Wei<sup>a,\*</sup>

<sup>a</sup> Centre for Water Technology (WATEC), Department of Biological and Chemical Engineering, Aarhus University, Universitetsbyen 36, 8000, Aarhus C, Denmark

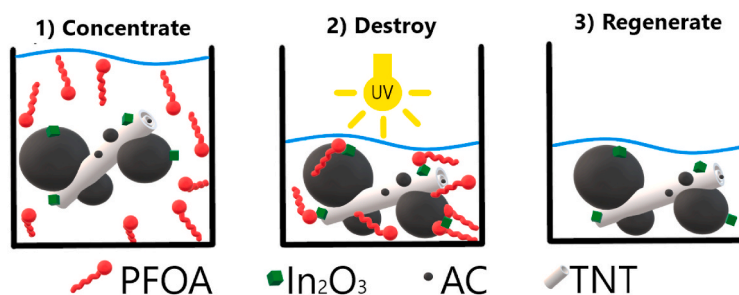
<sup>b</sup> Environmental Engineering Program, Department of Civil & Environmental Engineering, Auburn University, Auburn, AL, 36849, USA

<sup>c</sup> The Key Laboratory of Water and Sediment Sciences, Ministry of Education, College of Environmental Science and Engineering, Peking University, Beijing, 100871, China

## HIGHLIGHTS

- Adsorptive photocatalyst (In/TNT@AC) was prepared to concentrate-and-degrade PFOA.
- In/TNT@AC can adsorb PFOA from water and degrade it under UV irradiation.
- 2% Indium dopant enhanced adsorption and subsequent solid-phase degradation of PFOA.
- In promotes direct electron transfer from PFOA to the photogenerated hole ( $h^+$ ).
- The photodegradation also regenerates In/TNT@AC, allowing for repeated uses.

## GRAPHICAL ABSTRACT



## ARTICLE INFO

Handling Editor: Y Yeomin Yoon

### Keywords:

Concentrate-and-degrade

Perfluorooctanoic acid

Adsorptive photocatalyst

Heterojunction

Electron-hole recombination

## ABSTRACT

“Concentrate-and-degrade” is an effective strategy to promote mass transfer and degradation of pollutants in photocatalytic systems, yet suitable and cost-effective photocatalysts are required to practice the new concept. In this study, we doped a post-transition metal of Indium (In) on a novel composite adsorptive photocatalyst, activated carbon-supported titanate nanotubes (TNTs@AC), to effectively degrade perfluorooctanoic acid (PFOA). In/TNTs@AC exhibited both excellent PFOA adsorption (>99% in 30 min) and photodegradation (>99% in 4 h) under optimal conditions (25 °C, pH 7, 1 atm, 1 g/L catalyst, 0.1 mg/L PFOA, 254 nm). The heterojunction structure of the composite facilitated a cooperative adsorption mode of PFOA, i.e., binding of the carboxylic head group of PFOA to the metal oxide and attachment of the hydrophobic tail to AC. The resulting side-on adsorption mode facilitates the electron ( $e^-$ ) transfer from the carboxylic head to the photogenerated hole ( $h^+$ ), which was the major oxidant verified by scavenger tests. Furthermore, the presence of In enables direct electron transfer and facilitates the subsequent stepwise defluorination. Finally, In/TNTs@AC was amenable to repeated uses in four consecutive adsorption-photodegradation runs. The findings showed that adsorptive photocatalysts can be prepared by hybridization of carbon and photoactive semiconductors and the enabled

\* Corresponding author.

\*\* Corresponding author.

E-mail addresses: [zhaodon@auburn.edu](mailto:zhaodon@auburn.edu) (D. Zhao), [zwei@bce.au.dk](mailto:zwei@bce.au.dk) (Z. Wei).

<https://doi.org/10.1016/j.chemosphere.2022.134495>

Received 17 December 2021; Received in revised form 28 March 2022; Accepted 31 March 2022

Available online 4 April 2022

0045-6535/© 2022 The Author(s). Published by Elsevier Ltd. This is an open access article under the CC BY license (<http://creativecommons.org/licenses/by/4.0/>).

“concentrate-and-degrade” strategy is promising for the removal and degradation of trace levels of PFOA from polluted waters.

## 1. Introduction

Per- and polyfluoroalkyl substances (PFAS), a broad class of toxic and persistent chemicals (US EPA, 2021a; US EPA, 2021b), have been widely detected in the aquatic systems and are affecting the drinking water of millions of consumers in both Europe and North America (Backe et al., 2013; O’Connell et al., 2010; Rahman et al., 2014). The point sources for PFAS typically include firefighter training sites, landfill leachate, and even wastewater treatment plants. Once released to the environment, PFAS are highly resistant to biological processes and can accumulate and remain in the biota and human body over prolonged times. For example, perfluorooctane sulfonate (PFOS), one of the most prevalent PFAS, has a half-life of 41 years in the environment and 4–5 years in the human body (O’Connell et al., 2010). Mounting health research data have revealed that exposure to PFAS can lead to many health problems, such as thyroid hormone disruption, immune system impairment, and low infant birth weight (Jian et al., 2018). As a result, the United States Environmental Protection Agency (U.S. EPA) set the combined concentration of perfluorooctanoic acid (PFOA) and PFOS to 70 parts per trillion in drinking water (US EPA, 2022), and stringent enforceable regulations are underway in the U.S. and other countries.

The ever-increasing concern over PFAS has called for innovative low-cost and effective methods to remove and degrade these persistent organic pollutants (POPs) from water. Adsorption by activated carbon (AC) has been the most widely used method to remove PFAS owing to its low-cost operation and broad acceptability (Cantoni et al., 2021; Du et al., 2014; Park et al., 2020). In a field study, the 3M Company reported 98.4% removal of perfluorobutane sulfonic acid (PFBS) from its process effluent using granular activated carbon (GAC) (Minnesota Pollution Control Agency, 2009). Hydrophobic and anion- $\pi$  interactions between PFAS and AC have been found responsible for the adsorption (Saeidi et al., 2021). Yet, the hydrophobic interaction diminishes for shorter-chain PFAS. Further, regeneration of spent AC typically requires toxic, expensive organic solvents (e.g., methanol), inevitably producing a waste stream requiring additional treatments (Li et al., 2020a).

Advanced oxidation processes (AOPs) have been widely studied for PFAS degradation and removal from contaminated water. The strong C–F bond (536 kJ/mol), however, hindered the radical-based oxidation of PFAS molecules, particularly for hydroxyl radical ( $\bullet$ OH) which is reported to be inert to PFAS (Bentel et al., 2019). Various photocatalysts have been developed to promote the oxidative destruction of PFAS, such as TiO<sub>2</sub> (Li et al., 2016; Panchangam et al., 2009), In<sub>2</sub>O<sub>3</sub> (Li et al., 2013b), Ga<sub>2</sub>O<sub>3</sub> (Shao et al., 2013), and SiC/graphene (Huang et al., 2016). In general, photocatalytic degradation was found to follow a stepwise defluorination pathway (i.e., eliminate one –CF<sub>2</sub> in each reaction cycle (Gomez-Ruiz et al., 2018; Li et al., 2012b)). Although these photocatalysts can degrade PFAS to different extents, these photocatalysts were typically applied to treat bulk water, which often consumes excessive amounts of energy due to the large volumes treated. Moreover, the degradation intermediates (e.g., shorter-chain PFAS) remain in the treated water.

Recently, researchers have introduced a novel “Concentrate-and-Degrade” strategy to treat PFAS and other POPs using adsorptive photocatalysts (Li et al., 2020b; Qian et al., 2020, 2021; Zhu et al., 2021). Typically, low concentrations of PFAS from a large volume of water are pre-concentrated on an adsorptive photocatalyst and then photo-degraded with UV or solar light. Because the energy-intensive photo-degradation was only applied to the much smaller volume of the solids, this approach is expected to be more energy-efficient for treating bulk water (Li et al., 2020a). Typically, the adsorptive photocatalysts are prepared by combining photocatalysts with adsorbents such as AC,

zeolites, or carbon spheres, where the resulting heterojunctions (i.e., mixed phases or materials) show synergistic effects. On the one hand, the combined carbon and metal oxides enable multi-mechanism interactions with PFAS (complexation with the head group of PFAS and hydrophobic interaction with the tail group). The enhanced and selective adsorption of PFAS not only effectively concentrates the POPs on the photo-active surface sites but also mitigates the potential inhibitive effects of the raw water matrix. On the other hand, the carbon modification of the photocatalysts enhances light absorption, facilitates electron transfer, and inhibits electron-hole recombination, resulting in enhanced photocatalytic activity.

While iron (Li et al., 2020b; Xu et al., 2020) and gallium (Zhu et al., 2021) were tested as doping agents on different carbon-based materials to concentrate-and-degrade PFOA, Indium (In) with different nanostructures (Li et al., 2013b; Liu et al., 2021) is a promising alternative dopant to carbon composite materials (Li et al., 2013a) or metal oxides (Wu et al., 2019). Hence, in this study, we prepared an In modified AC-supported titanate nanotubes (In/TNTs@AC) to practice the “Concentrate-and-Degrade” strategy for enhanced degradation and removal of PFOA. The price of In and its scarcity are the factors preventing the full-scale application of this material, but the efficient solid-phase photodegradation of the pre-sorbed PFAS also regenerates the material, allowing for repeated uses of the In-doped material.

We hypothesized that post-transition metals (i.e., Indium), when deposited on TNTs@AC, can facilitate both adsorption and photocatalytic activity for PFOA. The cooperative adsorption due to both AC and In<sub>2</sub>O<sub>3</sub> not only shortens the spatial distance between the carboxylic head groups of PFOA and photo-generated electron holes but also results in a favorable molecular orientation for subsequent photocatalytic degradation reactions. The specific objectives were to: 1) prepare, optimize, and characterize In/TNTs@AC, 2) test the composite material for adsorption and photocatalytic defluorination of PFOA, 3) examine the stability of the material, and 4) elucidate the reaction pathway and underlying mechanisms. Results from this study could provide a basis to develop more cost-effective technologies for the removal and degradation of PFAS in both drinking water and wastewater.

## 2. Materials and methods

### 2.1. Chemicals and materials

P25 TiO<sub>2</sub> (80% anatase and 20% rutile) was purchased from Evonik (Worms, Germany) and was used as received. Granular sodium hydroxide was purchased from Acros Organics (Fair Lawn, NJ, USA), and indium nitrate, methanol, ethanol isopropanol, and PFOA were obtained from VWR International (Radnor, PA, USA). Indium oxide (In<sub>2</sub>O<sub>3</sub>) was purchased from Sigma Aldrich (Saint Louis, USA). Perfluoro-*n*-[1,2,3,4,5,6,7,8-<sup>13</sup>C<sub>8</sub>]octanoic acid (<sup>13</sup>C-PFOA or M8PFOA) was acquired from Wellington Laboratories Inc. (Guelph, Ontario, Canada) and was used as the isotopically labeled internal standards. All chemicals were of analytical grade or higher. Filtrasorb-400® GAC (F-400 GAC) made of bituminous coal was from Calgon Carbon Corporation (Pittsburgh, PA, USA). The GAC features a high density and high surface area for organic pollutant adsorption. All solutions were prepared using deionized (DI) water (18.2 M $\Omega$  cm, Millipore Co., USA). No PTFE containers were used in all experiments.

### 2.2. Synthesis and characterization of In/TNTs@AC

First, TNTs@AC was prepared following a prior alkaline hydrothermal method (Liu et al., 2016). Briefly, 1.2 g of TiO<sub>2</sub> and 2.4 g of AC were

dispersed in 67 mL of a NaOH solution (10M). The mixture was sealed and stirred overnight and then placed in an autoclave at 130 °C for 72 h. The solid was then separated and washed with a 10 wt% HCl solution, dried at 60 °C, and ground. Then, 1 g TNTs@AC was well dispersed in 100 mL of DI water and then modified by dropwise adding various amounts of a 0.1 M In(NO<sub>3</sub>)<sub>3</sub> solution (In-to-TNTs@AC = 0.5, 1, 2, 3, and 5 wt%). Upon adsorption equilibrium, which was checked by analyzing In<sup>3+</sup> remaining in the aqueous phase, the suspension was centrifuged and the material was transferred into a Petrie dish (using methanol as a dispersant), dried in an oven at 60 °C for 24 h, and ground. The obtained particles were calcined at 500 °C (temperature ramp = 250 °C/h) under a nitrogen flow (100 mL/min) in a tubular furnace (RSH 50/250/13 with a B410 controller and a gas supply system, Nabertherm GmbH, Lilienthal, Germany) for 4 h. Finally, the calcinated composite materials were rinsed with DI to remove the inorganic residuals, dried in an oven at 60 °C for 24 h, and ground. For comparison, In<sub>2</sub>O<sub>3</sub> was also directly loaded on AC by the same hydrothermal and calcination procedures.

### 2.3. Adsorption and photodegradation experiments

Batch adsorption tests were carried out at neutral pH in the dark. Adsorption kinetic experiments were initiated by adding 40 mL of a PFOA solution (100 µg/L) and 0.04 g of composite material in 40 mL amber glass vials. The µg/L level of PFOA was selected because such concentration has been identified at contamination sites. The mixtures were then capped and mixed on a tumbler at 50 rpm for 2 h, or until equilibrium. At predetermined time intervals (i.e., 30, 60, 120, and 240 min), selected vials were sampled and centrifuged at 2000 rpm for 5 min to separate the particles, and then an aliquot was taken from the supernatant and immediately filtered through a 0.22 µm polyether sulfones (PES) filter. The filtrate was then analyzed for PFOA and its degradation products. Adsorption isotherms were obtained with 2 g/L of catalyst and different PFOA concentrations ranging from 0.1 to 100 mg/L.

Following the adsorption of PFOA onto In/TNTs@AC, the suspension was left still for 1 h to allow the composite materials to settle by gravity (>99% of materials settled). Then, 35 mL of the supernatant was removed from the original 40 mL reaction solution, and the 5 mL residual solid-liquid mixture was transferred into a quartz dish reactor (volume = 50 mL; internal diameter = 4 cm) with a quartz cover. The internal diameter is an important factor to take into consideration since the irradiation surface can lead to a more effective light utilization avoiding screening factors. Next, 5 mL of MilliQ water was used to rinse the vial and then transferred to the quartz reactor. The resulting 10 mL of the solid-liquid mixture were subjected to UV irradiation (254 nm, light density = 2.28 mW/cm<sup>2</sup>) using a Rayonet chamber photo-reactor (Southern New England Ultraviolet CO, Branford, CT, USA). Agitation at 100 rpm was applied during the experiment to ensure contact between PFOA and the photocatalyst forming a thin dispersed layered suspension. At this point, the catalyst and PFOA concentrations are 4 g/L and 400 µg/L, respectively. The reactor was equipped with a ventilating fan to maintain the reactor temperature at around 25 °C.

During the photodegradation, samples were taken at predetermined time intervals (30, 60, 120, and 240 min). After filtering through 0.22 µm PES membrane filters, PFOA and its degradation products in the solid phase were extracted using 40 mL methanol at 80 °C for 4 h and analyzed; in the meantime, the filtrates were analyzed for PFOA, fluoride (F<sup>-</sup>), and other short-chain byproducts. The defluorination is defined as the quotient between the free fluoride detected in the solution after irradiation and the total fluoride atoms in the initial PFOA molecules in the solution (Eqn. (1)):

$$\text{Defluorination (\%)} = \frac{F^- \text{ atoms released in solution}}{F \text{ atoms in the PFOA molecules}} \times 100 \quad (1)$$

Effects of pH were tested by performing the photodegradation tests

in the initial pH range from 4.0 to 11.0. In addition, classical scavenger experiments were conducted to investigate the roles of h<sup>+</sup>, •OH, and O<sub>2</sub><sup>•-</sup> in the photocatalytic degradation of PFOA using potassium iodide (KI), isopropanol (ISP), and benzoquinone (BZQ), respectively (Li et al., 2020b). The robustness and reusability of In/TNTs@AC were examined by reusing the material in 4 consecutive cycles.

### 2.4. Analytical methods

The surface morphology of In/TNTs@AC was imaged using a scanning electron microscope (SEM) (20 kV, FEI XL30F, Philips, USA), equipped with energy-dispersive X-ray spectroscopy (EDS) and transmission electron microscopy (TEM) (Tecnai™ Spirit, UK). The particle size distribution of the materials was measured by a Dynamic Light Scattering (DLS) Sizer (Malvern Zetasizer Nanoseries ZS, UK). The crystalline structures were analyzed by a Bruker X-ray diffractometer (XRD, D2 PHASER, Bruker AXS, Germany) with Cu Kα radiation (λ = 1.5418 Å) and at a scanning rate (2θ) of 2° min<sup>-1</sup>. Zeta potential was measured by a Malvern Zetasizer Nano-ZS90 (Malvern Instrument, Worcestershire, UK) sampling the supernatant of the materials dispersed in water, while the surface chemical compositions, along with oxidation states, were measured with an AXIS-Ultra X-ray photoelectron spectroscopy (XPS) (Kratos, England, 15 kV and 15 mA (Al Kα X-ray) using the standard C 1s peak (Binding energy, Eb = 284.80 eV) for calibration and elimination of static charge effects. During the measurements, the chamber pressure was kept below 5 × 10<sup>-9</sup> mbar. The results were confirmed by Fourier-transform infrared spectroscopy (FTIR) (Vertex 70V, Denmark). Light absorption was evaluated using a Thermo Scientific UV/Vis Spectrophotometer (Genesys 150, Denmark). The p-n nature of the photocatalyst was evaluated with a CHI760E Electrochemical Analyzer (CH Instruments, USA). The specific surface area was measured using an ASAP 2010 Brunauer–Emmett–Teller (BET) surface area analyzer (Micromeritics, USA). The pore size distribution and pore volumes were determined via the Barret–Joyner–Halender (BJH) method and nitrogen adsorption method at the relative pressure of 0.99, respectively.

Aqueous PFOA and degradation intermediates were analyzed using an ultra-performance LC system (UPLC, ACQUITY, Waters Corp., USA) coupled with a quadrupole time-of-flight mass spectrometer (QTOF/MS, Q-ToF Premier, Waters) and electrospray ionization (ESI) in the negative mode. In the analysis, 20 µg/L of internal standard were added following the photodegradation experiments to ensure the reproducibility of the measurements (>90% PFOA recovery in duplicated tests). The instrument detection limit was 100 ng L<sup>-1</sup>. Fluoride in the aqueous phase was analyzed using an ion chromatography (IC) system (Dionex Aquion, CA, USA) with an IonPac AS23 IC column (Dionex). The injection loop was 25 µL and the flow rate was set at 0.25 mL/min. The eluent was prepared by diluting a sodium carbonate and sodium bicarbonate concentrate (ThermoScientific, Denmark) to 4.5 mM and 0.8 mM, respectively. Dissolved In and Ti in the sample supernatant during catalyst synthesis and after the reaction was measured with an inductively coupled plasma-optical emission spectroscopy (ICP-OES, 710-ES, Varian, USA).

## 3. Results and discussion

### 3.1. Characterization of In/TNTs@AC

The morphology and microscopic structure of as-prepared In/TNTs@AC were characterized. The SEM images (Fig. 1a) displayed a cotton-like structure mingled with carbon and titanate nanotubes (TNTs). Meanwhile, the EDS spectra (Fig. 1b) confirmed five major elements (C, O, Na, In, and Ti) on the surface of In/TNTs@AC (Table S1), indicating In was successfully loaded on the surface of TNTs@AC. The TEM images (Fig. 1c and d) indicate the clusters of TNTs (red circle) appeared as an interwoven network spreading all over the surface, suggesting co-growth of TNTs and nanosized AC particles. Free AC

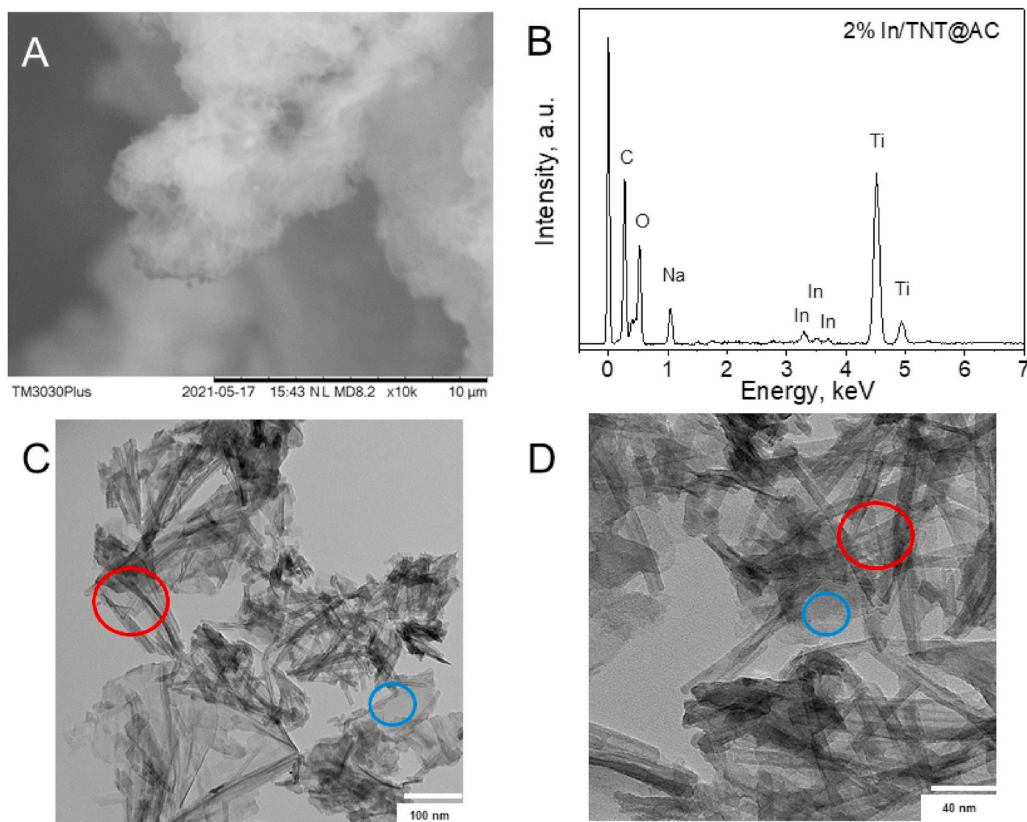


Fig. 1. (a) SEM image, (b) EDS analysis, (c and d) TEM images of In/TNTs@AC (red circle: clusters of TNTs appeared as an interwoven network; blue circle: AC exhibited a flat, smooth, and bulky structure like a terraced field). (For interpretation of the references to colour in this figure legend, the reader is referred to the Web version of this article.)

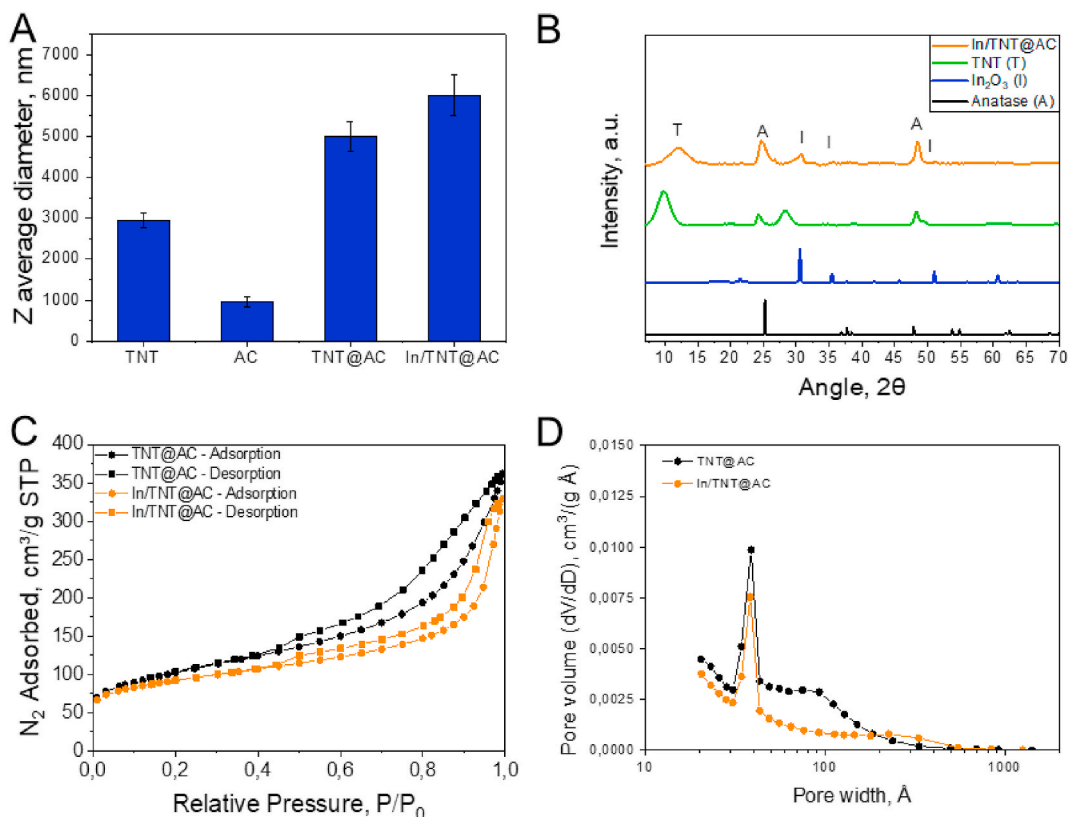


Fig. 2. (a) Particle size analysis, (b) XRD patterns High resolution, (c) N<sub>2</sub> adsorption-desorption isotherms, and (d) pore size distributions of different materials.

microparticles might also be found in the material. Image processing of 10 random nanotubes using ImageJ software confirms that the average outer diameter of the tubes is  $(7.8 \pm 1.0)$  nm, which agrees with the reported value by Liu et al. (2016). As a comparison, the parent AC (F-400) exhibited a flat, smooth, and bulky structure like a terraced field (blue circle). The largest particle size distribution of In/TNT@AC suggests the effective binding of the different composite materials, indicating a better sedimentation capability of the composite material against the pristine components of the composite due to the heavier aggregates formed during the hydrothermal and the calcination processes (Fig. 2a).

Consistent with the EDS results, the XRD diffractograms for synthesized In/TNTs@AC, TNT alone, calculated anatase, and commercial  $\text{In}_2\text{O}_3$  (Fig. 2b) also indicate the successful loading of In on TNTs@AC. The peaks at  $22^\circ$ ,  $31^\circ$ ,  $35^\circ$ ,  $42^\circ$ ,  $46^\circ$  are assigned to the indium oxide ( $\text{In}_2\text{O}_3$ ). The diffraction peaks of TNT uncalcined at  $10.0^\circ$ ,  $24.5^\circ$ ,  $28.6^\circ$ ,  $48.5^\circ$  correspond to the (2 0 0), (1 1 0), (3 1 0), (0 2 0) planes of the titanate structure. The (2 0 0) peak decreased and moved to  $12.0^\circ$  for In/TNT@AC, indicating the decrease of the interlayer of TNT (Jiang et al., 2012). A small peak at  $27^\circ$  is assigned to the crystal planes (002) of graphite (Le et al., 2012; Rey et al., 2012). The presence of AC suggests that the surface of the photocatalysts is possibly grafted with some micro-carbon particles (Dang et al., 2020). This observation is consistent with our previous result that, after calcination, titanate was transformed to anatase on the catalyst surface of the TNTs@AC. The FTIR data (Fig. S1) shows a decrease in the bands at  $\sim 3000$ – $3600$  and  $\sim 1600$ – $1750$   $\text{cm}^{-1}$  after the calcination. The bands correspond to alcohol, carboxyl, and carbonyl groups, respectively (Wang et al., 2018). Therefore, the results indicate the removal of these functional groups, which can lead to a decrease in the density of negative charge at near-neutral pH for carbonaceous materials (Ogata et al., 2020; Wang and Chen, 2015) favoring the interactions between the composite and PFOA.

The pore size is a critical factor that influences the intraparticle diffusion of PFOA in In/TNTs@AC. Fig. 2c showed a type IV isotherm for TNT@AC and In/TNT@AC, suggesting mesoporosity (Liu et al., 2016). The materials also exhibit a pore volume reduction from  $0.55$   $\text{cm}^3/\text{g}$  to  $0.51$   $\text{cm}^3/\text{g}$  upon loading of In onto TNTs@AC. Fig. 2d presents similar bimodal pore size distribution for both TNTs@AC and In/TNTs@AC with a peak at  $\sim 4$  nm, though In/TNTs@AC demonstrated a reduction in  $dV/dD$  in the range of 5–20 nm compared with TNTs@AC. The In doping and calcination appears to narrow or even block some interior pores of the AC, which, may favor the adsorption of PFOA on the outer shell of In/TNTs@AC and hence the subsequent photodegradation. The impact of pore size variation was further verified in the subsequent adsorption tests.

The XPS survey spectra (Fig. 3a) also confirmed the successful addition of In on In/TNTs@AC, with C, Na, Ti, O, and In being the main elements on the material surface. Fig. 3b shows the high-resolution XPS spectra centered on Ti 2p, where the two peaks at 459.4 and 465.2 eV correspond to the orbitals  $2p_{1/2}$  and  $2p_{3/2}$ , respectively. The splitting energy was 5.8 eV, which confirmed  $\text{Ti}^{4+}$  was the major titanium form (5.7–5.9 eV) (Hong et al., 2013). In addition, the absence of the peak at 457 eV indicated that no  $\text{Ti}^{3+}$  was present (Qianqian et al., 2011). An additional deconvoluted peak appeared at 461 eV for TNTs@AC corresponding to the C–Ti bond formed during the hydrothermal treatment (Hong et al., 2013). Moreover, the peak at 452.1 eV for In/TNTs@AC belongs to the deconvoluted spectra of In, corresponding to the  $3d_{3/2}$  orbital (Gayen et al., 2012; Nguyen et al., 2021). A shoulder appears from 454 to 456 eV, which can be deconvoluted into two peaks. The first has a binding energy of 454 eV corresponding to In(0) (Lin et al., 1977) from the calcination under the  $\text{N}_2$  atmosphere. The transition from In(0) to  $\text{In}_2\text{O}_3$  occurs after exposure to atmospheric conditions (Detweiler et al., 2016). The presence of  $\text{In}_2\text{O}_3$  and a minor fraction of In(0) after the calcination of In/TNT@AC has also been reported elsewhere under similar anoxic calcination conditions (Soares et al., 2021). The

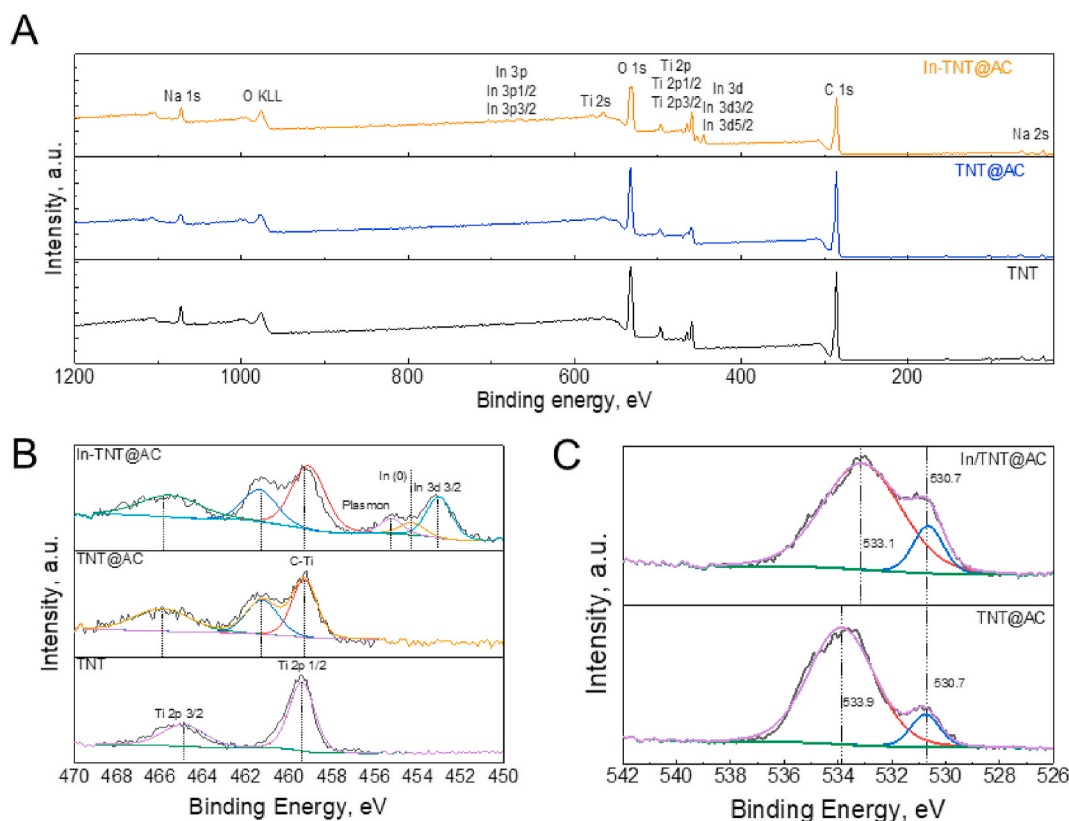


Fig. 3. (a) Full XPS spectrum, (b) High resolution Ti 2p spectra, (c) High resolution C 1s spectra.

additional peak at 455 eV corresponds to a plasmon energy loss from the orbital  $3d_{5/2}$  in accordance with previous studies (Detweiler et al., 2016; Lin et al., 1977).

Fig. 3c shows the high-resolution deconvoluted spectra of O 1s. For In/TNTs@AC, a peak at 530.7 eV appeared, which corresponds to the Ti–O–Ti ( $Ti^{4+}$ ) lattice structure of TNTs, while another peak at 533.9 eV indicates the Ti–OH surface groups (Dang et al., 2020). Notably, the addition of indium shifted the peak to 533.1 eV, suggesting the doping of In in the material surface and the formation of oxygen vacancies (Ma et al., 2021). Fig. S2 shows the C 1s high-resolution spectra. The peaks at 284.3, 284.9, 286.4, and 289 eV are assigned to the calibration background C–C/C–H, C–O, C=O, and  $\pi$ – $\pi$ , respectively (Dang et al., 2020). Moreover, the relative increase of the C–O peak concerning C=O also suggests the formation of oxygen vacancies and successful incorporation of In in the TNT@AC composite material. In addition, the Mott-Schottky plot for synthesized TNT and commercial  $In_2O_3$  confirmed the n-type nature of the photocatalysts (Fig. S3).

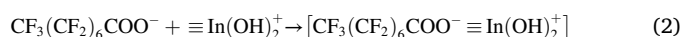
### 3.2. Adsorption of PFOA

Batch adsorption tests were carried out to gauge the adsorption rate and capacity of In/TNTs@AC as compared with the parent materials AC and TNTs@AC. Fig. S4 shows that 2% In-doped TNTs@AC exhibited the highest defluorination rate, and was thus selected in the subsequent adsorption and photodegradation tests. Fig. 4a shows that >99% removal of PFOA was achieved by 2% In/TNTs@AC after 30 min, and the adsorption equilibrium was reached within 30 min, which is much faster than the parent AC (120 min) and TNTs@AC (~90% at >240 min). The fast PFOA adsorption on In/TNTs@AC suggests that the rate limit step was likely the surface interaction rather than molecule diffusion into the porous structures of composite materials. This is in line with the postulate that some of the deep sites in the carbon core were blocked upon the alkaline hydrothermal treatment (Liu et al., 2016). As a result, most PFAS are favored to be concentrated on the more

photoactive outer-shell sites. The adsorption amount of PFOA was more than 20% higher for In/TNTs@AC than that of TNTs@AC after 240 min (Fig. 4b), indicating the addition of In promoted the capture of PFOA.

The adsorption isotherm is well-fitted to the Freundlich Model (Singh, 2016) (Fig. S5). The Freundlich equation (Eqn. S(1)) can apply to highly heterogeneous surfaces, such as In/TNT@AC, and the lack of a clear plateau indicates that multilayered adsorption occurs (Jasper et al., 2020). Table S2 provides the values of the adsorption limit (Kf) and adsorption density (n) for TNT@AC and In/TNT@AC.

PFOA adsorption on AC-based materials is attributed to hydrophobic and electrostatic interactions (Wei et al., 2019). Given the dual-functional characteristics of PFOA, namely, the negatively charged head carboxylate group and the hydrophobic “tail group” ( $-CF_3(CF_2)_6$  group), PFOA can strongly interact with the hydrophobic “micro carbon” particles on In/TNTs@AC; moreover, the positively charged  $In_2O_3$  catalyst ( $pH_{PZC} = 8.7$ ) (Kosmulski, 2001) can interact with the carboxylate group through both electrostatic and Lewis acid-base interactions (Eqn. (2)), resulting in enhanced adsorption selectivity. Fig. 4c demonstrates that the addition of In onto TNTs@AC has shifted the point of zero charge (PZC) from about pH 3 (TNTs@AC) to pH 4 (In/TNTs@AC). It can be expected that more PFOA would be concentrated at the local  $In_2O_3$  sites, where a heterojunction structure of carbon- $In_2O_3$  and  $TiO_2$ - $In_2O_3$  exists providing multiple adsorption mechanisms.



At the molecular level, both In and micro carbon particles could control the adsorption of PFOA anions by altering their spatial orientation, *i.e.*, “vertical adsorption” or “parallel adsorption” on the surface of the composite materials (Li et al., 2020b). The combined interactions from  $In_2O_3$  (for hydrophilic head) and carbon (for hydrophobic tail) can result in the dual adsorption modes that facilitate stronger binding of PFOA onto the photocatalyst surface and thus shorten the distance between PFOA and photo-generated  $h^+$  or  $e^-$  on TNTs for improved PFOA decomposition and mineralization.

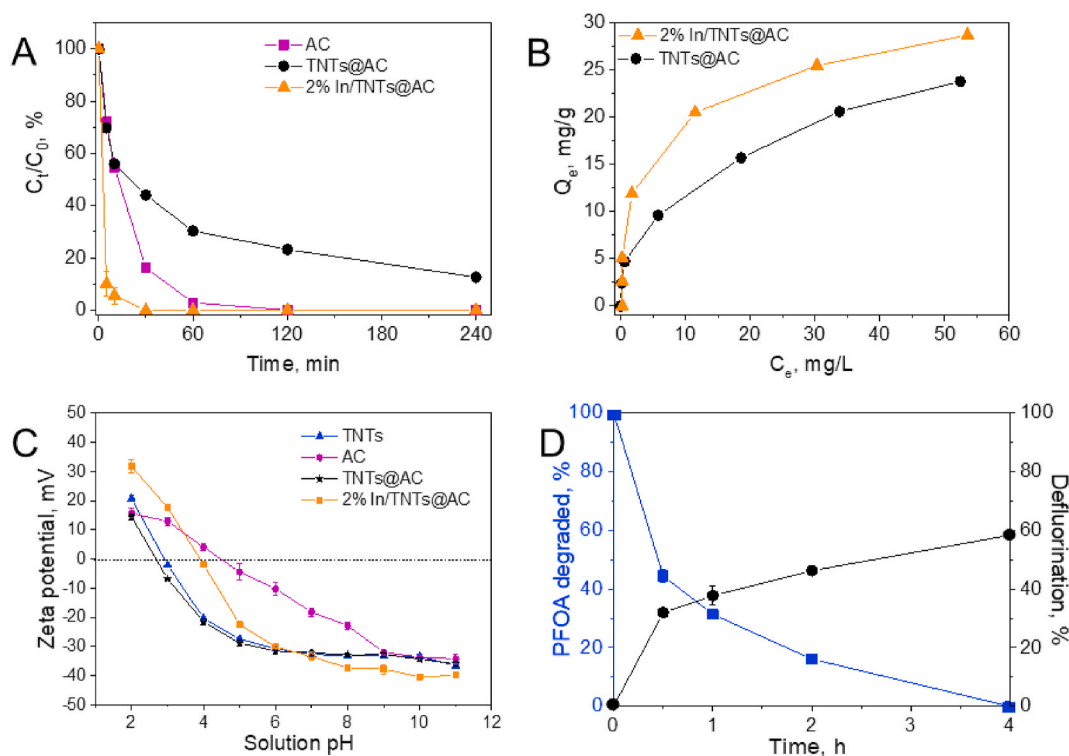


Fig. 4. (a) PFOA adsorption kinetics, (b) PFOA adsorption isotherms, (c) Zeta potential of different materials at different pH levels and (d) Photodegradation (In/TNTs@AC doped with 2 wt% In). Catalyst dose =  $1 \text{ g L}^{-1}$ ; (a) [PFOA] =  $100 \mu\text{g L}^{-1}$ ; (b) [PFOA] = from  $100 \mu\text{g L}^{-1}$  to  $100 \text{ mg L}^{-1}$ ; catalyst dose =  $2 \text{ g L}^{-1}$  and (d) concentrate and degrade; [PFOA] initial =  $100 \mu\text{g L}^{-1}$ ; 254 nm.

### 3.3. Photodegradation of PFOA

Upon UV irradiation, free electrons are produced on TNTs surfaces along with the electron holes. As shown in Fig. 4d, PFOA pre-sorbed on In/TNTs@AC was rapidly photodegraded (over 50% in 30 min). After 4 h UV irradiation, PFOA was nearly completely degraded by In/TNTs@AC, and ~60% defluorination of PFOA was observed. No pH change occurs during the reaction. Fig. 5a compares the 4 h of photocatalytic defluorination extents of PFOA by different materials: AC, TNTs@AC, In<sub>2</sub>O<sub>3</sub>@AC, and In/TNTs@AC. In/TNTs@AC not only far exceeded the parent AC and TNTs@AC but also defluorinated ~33% more PFOA compared with In<sub>2</sub>O<sub>3</sub>@AC. Note that the screening effect can be dramatic when decreasing the irradiation surface, increasing the catalyst dosage, or introducing additional particles in the reaction suspension. The higher content of nontransparent material used in the synthesis may also challenge the photocatalytic efficiency.

It is well known that AC alone offers little photoactivity. While TNTs@AC is expected to offer greater PFOA degradation than parent TiO<sub>2</sub> (Liu et al., 2016), however, the negative surface potential of TNTs creates an unfavorable condition for the adsorption and degradation of PFOA anions. The degradation efficiency of PFOA is increased by In<sub>2</sub>O<sub>3</sub>@AC since it also presents a dual adsorption mechanism. However, the highest defluorination efficiency is obtained when doping In onto TNT@AC. Such a synergistic combination ensures both high-efficient adsorption and high electron-hole availability due to the formation of heterojunctions for electron trapping.

The pre-concentration of PFOA on In/TNTs@AC through strong hydrophobic and electrostatic interactions played a critical role in the enhanced degradation of PFOA and the high defluorination rate. The effective photocatalytic degradation of PFOA by In/TNTs@AC could be attributed to the direct hole oxidation of sorbed PFOA on the material surface (Li et al., 2012a). Li et al. reported that the reaction between

holes and PFOA is faster than the production of hydroxyl radicals from the holes according to electron spin resonance analysis (Li et al., 2012a). The presence of AC also facilitates the transfer of photo-generated electrons, which inhibits the recombination of the photo-generated holes and electrons. The presence of In on the material surface played several important roles (Section 3.4). Additionally, material calcination is also important. The UV-Vis tests indicated an increase in the absorption maximum for calcined samples along with a red-shift of the spectrum (Fig. S6a), which increases the photocatalytic response of the catalyst. The bandgap of the doped-catalyst decreased according to the TAUC plot (Fig. S6b) from ~3.4 to ~3 eV after the calcination process facilitating the electron excitation and thus the photocatalytic activity. Prior work showed that the calcination transformed titanate into anatase for a broader range of light absorption (Li et al., 2020b). However, over calcination should be avoided because titanate could transform into rutile that is less photo-sensitive compared with anatase.

Fig. 5b shows the initial pH effect on the PFOA defluorination. The photocatalytic defluorination decreased with increasing solution pH, reaching ~45% defluorination at pH ≥ 9 in 4 h. The observation can be attributed to: 1) the material surface becomes more negative at higher pH, decreasing the adsorption of PFOA anions and subsequent photodegradation; and 2) while the photo-generated holes played a critical role in the degradation of PFOA, more holes were consumed by the competitive conversion of OH<sup>-</sup> to •OH at elevated pH (Lawless et al., 1991). Thus, neutral or acidic conditions are suggested for PFOA photodegradation by In/TNTs@AC.

The classical scavenger quenching experiments were carried out to scrutinize the roles of h<sup>+</sup>, •OH, and O<sub>2</sub><sup>•-</sup> in the PFOA photodegradation by In/TNTs@AC (Fig. 5c). Specifically, KI, ISP, and BZQ were assigned as scavengers (Li et al., 2018; Wei et al., 2017) for both h<sup>+</sup> and •OH ( $k \geq 1.1 \times 10^{10} \text{ M}^{-1} \text{ s}^{-1}$ ) (Buxton et al., 1988), •OH ( $k = 1.9 \times 10^9 \text{ M}^{-1} \text{ s}^{-1}$ ) (Buxton et al., 1988), and O<sub>2</sub><sup>•-</sup> ( $k = 3.7 \times 10^6 \text{ M}^{-1} \text{ s}^{-1}$ ) (Sawada et al.,

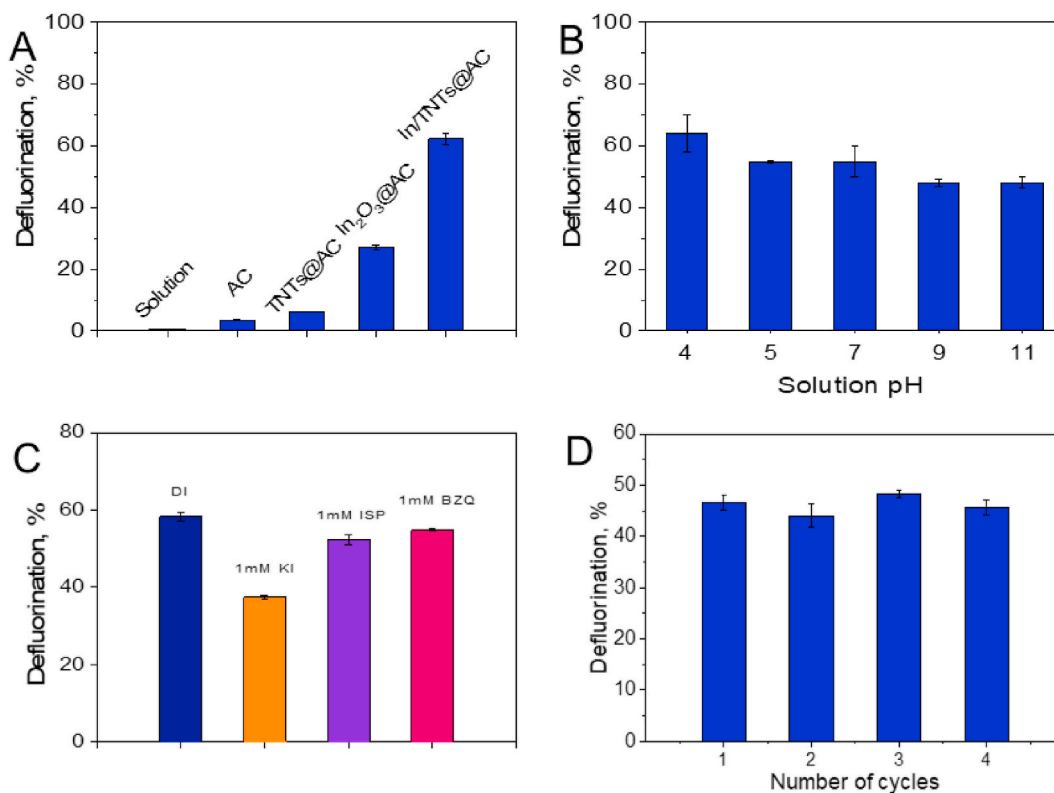


Fig. 5. (a) Defluorination of PFOA by different composite materials, (b) Effects of pH on PFOA defluorination, (c) Effects of various scavengers on defluorination of PFOA pre-sorbed on In/TNTs@AC, (d) Reusability test on PFOA. Experimental conditions of the concentration stage: initial [PFOA] = 100  $\mu\text{g L}^{-1}$ , material dosage = 1.0 g  $\text{L}^{-1}$ , solution volume = 40 mL concentrated and degraded, reaction time = 4 h, and pH = 7.0  $\pm$  0.3; (c) KI, ISP, and BZQ concentration = 1 mM.

1975), respectively. The addition of 1 mM KI reduced the defluorination from 58% to 37% at neutral pH. In comparison, the presence of ISP only slightly inhibited the PFOA defluorination to 52%, and BZQ showed negligible changes. The results suggest that  $h^+$ -induced oxidation played a dominant role in the defluorination reactions in this study. These results are consistent with our previous observation, i.e.,  $h^+$ -facilitated oxidation was the key degradation mechanism for PFOA in the photocatalytic system (Li et al., 2013b; Vecitis et al., 2009). In addition, the low defluorination observed by TNT@AC and the heterojunction formed between metal oxides (Section 3.4) indicate the higher effectiveness of  $\text{In}_2\text{O}_3$  holes compared to  $\text{TiO}_2$ .

### 3.4. Photodegradation pathway of PFOA

Based on the experimental findings and the literature, the photocatalytic degradation pathway of PFOA by In/TNTs@AC is proposed. It is described that  $\text{In}_2\text{O}_3$  holes can rapidly react with PFOA due to their bidentate adsorption mechanism (Li et al., 2012a). TNT holes preferentially react with  $\text{OH}^-$  and  $\text{H}_2\text{O}$  to produce  $\cdot\text{OH}$  (Eqns. 3-4) (Li et al., 2012a), which are used in subsequent steps. In addition, the reported band values of  $\text{In}_2\text{O}_3$  and anatase  $\text{TiO}_2$  (Song et al., 2017) permit the formation of a type-II heterojunction to promote electron-hole availability according to Fig. 6a.

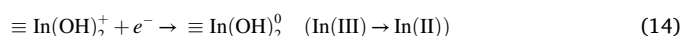
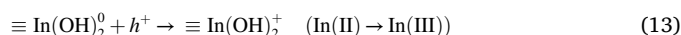
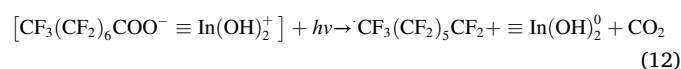
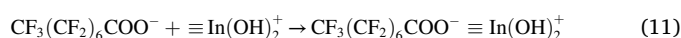


First,  $h^+$  is photogenerated and available at the valence band (VB) of  $\text{In}_2\text{O}_3$  when  $e^-$  jumps over to the conduction band (CB; Eqn. (5)) on TNTs. Then,  $h^+$  withdrew one free electron from PFOA anion ( $\text{CF}_3(\text{CF}_2)_6\text{COO}^-$ ) to form a perfluoroalkyl radical ( $\text{CF}_3(\text{CF}_2)_5\text{CF}_2\text{COO}\cdot$ ) (Eqn. (6)), which is unstable and undergoes Kolbe-like decarboxylation reaction to give  $\cdot\text{CF}_3(\text{CF}_2)_5\text{CF}_2$  (Eqn. (7)). Upon reaction with generated  $\cdot\text{OH}$ ,  $\cdot\text{CF}_3(\text{CF}_2)_5\text{CF}_2$  loses a "CF<sub>2</sub> group" and releases  $\text{F}^-$  ions (Eqn. (8)–(10)) (Panchangam et al., 2018; Peng et al., 2017). The resulting  $\text{C}_6\text{F}_{13}\text{COO}^-$  may undergo a second cycle of degradation, each losing a "CF<sub>2</sub>" unit, until complete defluorination.



This stepwise chain-shortening reaction pathway was verified through the analysis of the reaction intermediates (Fig. S7). After 2 h of the UV photodegradation, the  $m/z$  peaks of PFOA and its intermediates were mainly located at 413 for PFOA anions, 363 for perfluoroheptanoic anion (PFHpA-,  $\text{C}_7\text{F}_{13}\text{O}_2^-$ ), 313 for perfluorohexanoic anion (PFHxA-,  $\text{C}_6\text{F}_{11}\text{O}_2^-$ ), 263 for perfluorovaleric anion (PFPEA-,  $\text{C}_5\text{F}_9\text{O}_2^-$ ), 213 for perfluorobutyric anion (PFBA-,  $\text{C}_4\text{F}_7\text{O}_2^-$ ), 163 for pentafluoropropionic anion (PFPA-,  $\text{C}_3\text{F}_5\text{O}_2^-$ ), and 113 for trifluoroacetic anion (TFA-,  $\text{C}_2\text{F}_3\text{O}_2^-$ ). Other polyfluorinated intermediates corresponding to partial  $\text{CF}_2$  defluorinated units and extremely unstable intermediates (such as  $\text{C}_n\text{F}_{2n+1}\text{OH}$  and  $\text{C}_n\text{F}_{2n}\text{O}$ ) were not identified. Tang et al. (2012) and Chen et al. (2007) reported similar intermediates in the photodegradation process of PFOA. The stronger PFHxA peak in the mass spectrum, after 2 h supports the dual adsorption mechanism of the composite. PFOA is intensively degraded due to its hydrophobic interactions with AC and higher affinity for the locally positively charged  $\text{In}_2\text{O}_3$  (especially for short-chain TFA anions with high hydrophilicity).

The presence of In could create a new redox cycle and route for PFOA degradation on the In/TNTs@AC surface (Li et al., 2012a). The complexation of PFOA and In (Eqn. (11)) enables direct electron transfer from the PFOA carboxylate group to In(III) yielding  $\cdot\text{CF}_3(\text{CF}_2)_5\text{CF}_2$ ,  $\equiv\text{In}(\text{OH})_2^0$ , and  $\text{CO}_2$  (Eqn. (12)). Then, In(II) can be oxidized to In(III) by holes ( $h^+$ ) (Eqn. (13)). Meanwhile, In(III) can also trap the photogenerated  $e^-$  to form In(II) (Eqn. (14)). The results from Fig. 5a indicate that the In-facilitated redox cycle played a crucial role in the PFOA photodegradation (also Fig. 6b).



The dissolved oxygen is reported to react with the photogenerated electrons and the electrons on the oxygen vacancies of the catalyst to produce superoxide radicals which can react with PFOA through nucleophilic attack of the C–F bond and decarboxylate PFOA (Javed et al., 2020). However, the scavenger tests (Fig. 5c) suggest negligible effect from superoxide radicals. In addition, the reactivity of  $\text{O}_2^{\cdot-}$  is also reported to be hindered by the strong solvation by  $\text{H}_2\text{O}$  molecules which limits its reactivity towards PFOA (Javed et al., 2020), the presence of the quartz cover on the beaker might also prevent the oxygen passage into the reaction volume hindering this reaction.

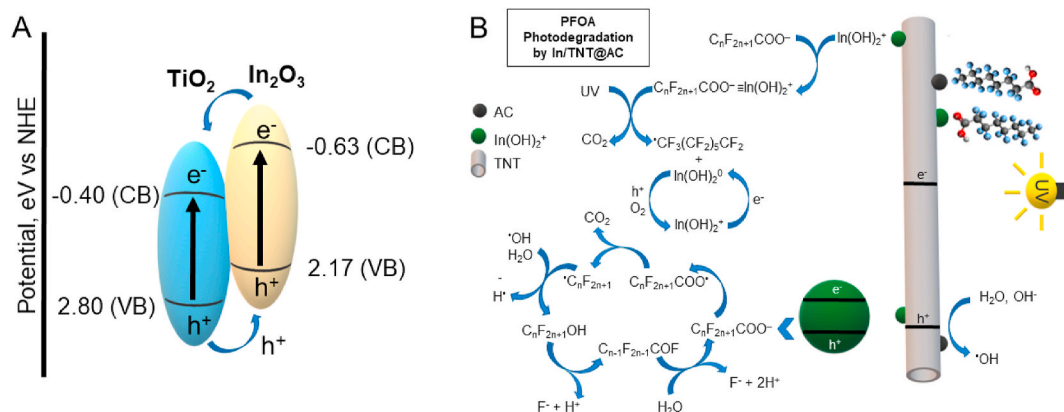


Fig. 6. (a) Electron-hole recombination of  $\text{In}_2\text{O}_3$  and anatase type-II heterojunction based on reported VB and CB values (Song et al., 2017), (b) Schematic diagram of PFOA photodegradation by In/TNT@AC composite material.

In summary, the doped In has brought several advantages to the photocatalytic system: 1) it creates local positively charged sites for vertical PFOA adsorption to enhance the photodegradation; 2) In may directly interact with the carboxylate group of POFA, resulting in a head-on adsorption mode that is conducive to the subsequent cleavage of the terminal  $\text{COO}^-$  group of PFOA, 3) the In/TNT@AC can trap  $e^-$  to avoid its recombination with  $h^+$ , and 4) the partial replacement of  $\text{In}^{3+}$  for  $\text{Ti}^{4+}$  in titanate may result in oxygen vacancies that can facilitate separation of  $e^-$  and  $h^+$  (Zhu et al., 2021). The presence of In induces a pathway in which PFOA directly reacts with photogenerated  $h^+$  (Li et al., 2013a, 2013b), which is different from the traditional photocatalytic reaction where  $h^+$  reacts with  $\text{H}_2\text{O}$  to generate  $\bullet\text{OH}$  that is inert to PFAS molecules.

### 3.5. Stability of the photocatalyst

The stability and reusability of a photocatalyst are important factors for engineering applications. The reusability of In/TNTs@AC was tested in four consecutive cycles of adsorption and photo-regeneration. Fig. 5d shows that In/TNTs@AC exhibits no noticeable defluorination efficiency loss. In addition, the robustness of In/TNTs@AC was tested over a broad range of initial pH (4–11) (Fig. 5b). The adsorption capacity of In/TNTs@AC was not influenced by over 99% PFOA adsorption in the tested pH range, while the defluorination remained >40% even at alkaline pH. The performance confirmed the robust physical integrity and chemical stability for In/TNTs@AC. Finally, high indium usage was observed regardless of the In doping percentage (Fig. S8). The In percentage remaining in the solution after photodegradation is below 1% for the 2% In/TNT@AC catalyst due to the high adsorption of In cation in the negatively charged TNT@AC. The high stability prevents secondary waste generation and the need for extra treatment stages for metal removal (Arana Juve et al., 2022).

## 4. Conclusions

A “concentrate-and-degrade” strategy was tested using an adsorptive photocatalyst (In/TNTs@AC) to simultaneously promote mass transfer and photodegradation efficiency of PFOA on the catalyst surface. In/TNTs@AC was designed to serve two purposes: 1) rapidly concentrate PFOA on the photoactive sites through adsorption onto AC, AC-amended TNTs, and positively charged  $\text{In}_2\text{O}_3$  particles, shortening the spatial distance between photogenerated  $h^+$  and PFOA; and 2) degrade the pre-adsorbed PFOA through photo-generated holes via the stepwise defluorination pathway, which was initiated by decarboxylation of the carboxylate head group of PFOA.

Although In/TNTs@AC exhibited promising adsorption and photodegradation performances, some critical issues still need to be addressed to realize the “concentrate-and-degrade” concept. The following perspectives may be taken into consideration to scale up the technology:

- 1) It is recommended in future efforts to investigate the effects of water matrices including dissolved organic matter, inorganic cations (e.g.,  $\text{Mg}^{2+}$ ,  $\text{Ca}^{2+}$ , and  $\text{Fe}^{3+}$ ), and co-pollutants.
- 2) Moreover, suitable engineering designs are desired to retrofit the In/TNTs@AC-based processes into current wastewater treatment systems. In addition to the combined treatment train of adsorption-sedimentation-degradation, different technologies can be coupled for continuous treatment of the PFAS contaminated water (i.e. a functionalized membrane with photocatalysts).
- 3) Finally, an economic assessment of the “concentrate-and-degrade” approach is of great importance to developing more cost-effective and eco-friendly technologies for treating PFAS and other POPs in waters.

## Author contributions statement

Jan-Max Arana Juve performed experiments and wrote the first draft; Fan Li, Yangmo Zhu, and Wen Liu helped data collection and analysis and revised the manuscript; Lars D.M. Ottosen supervised the students and revised the manuscript; Dongye Zhao and Zongsu Wei initiated the idea, secured funding, supervised the students, and wrote the manuscript.

## Declaration of competing interest

The authors declare that they have no known competing financial interests or personal relationships that could have appeared to influence the work reported in this paper.

## Acknowledgments

This work was partially funded by Aarhus University Centre for Water Technology (AU-WATEC) Start-Up Fund from Grundfos Foundation, Aarhus University Research Foundation Starting Grant (AUFF-E-2019-7-28), Novo Nordisk Foundation (NNF20OC0064799), and the U.S. Strategic Environmental Research and Development Program (SERDP) (ER18–1515 and ER19-1422). We are grateful to Dr. Andrea Leeson, Ms. Cara Patton, and Ms. Amy Maples of SERDP for their valuable technical advice and administrative assistance.

## Appendix A. Supplementary data

Supplementary data to this article can be found online at <https://doi.org/10.1016/j.chemosphere.2022.134495>.

## References

- Arana Juve, J.M., Christensen, F.M.S., Wang, Y., Wei, Z., 2022. Electrodialysis for metal removal and recovery: a review. *Chem. Eng. J.* 435, 134857. <https://doi.org/10.1016/j.cej.2022.134857>.
- Backe, W.J., Day, T.C., Field, J.A., 2013. Zwitterionic, cationic, and anionic fluorinated chemicals in aqueous film forming foam formulations and groundwater from U.S. military bases by nonaqueous large-volume injection HPLC-MS/MS. *Environ. Sci. Technol.* 47, 5226–5234. <https://doi.org/10.1021/es3034999>.
- Bentel, M.J., Yu, Y., Xu, L., Li, Z., Wong, B.M., Men, Y., Liu, J., 2019. Defluorination of per- and polyfluoroalkyl substances (PFASs) with hydrated electrons: structural dependence and implications to PFAS remediation and management. *Environ. Sci. Technol.* 53, 3718–3728. <https://doi.org/10.1021/acs.est.8b06648>.
- Buxton, G.V., Greenstock, C.L., Helman, W.P., Ross, A.B., 1988. Critical Review of rate constants for reactions of hydrated electrons, hydrogen atoms and hydroxyl radicals ( $\bullet\text{OH}/\bullet\text{O}^-$ ) in Aqueous Solution. *J. Phys. Chem. Ref. Data* 17, 513–886. <https://doi.org/10.1063/1.555805>.
- Cantoni, B., Turolla, A., Wellmitz, J., Ruhl, A.S., Antonelli, M., 2021. Perfluoroalkyl substances (PFAS) adsorption in drinking water by granular activated carbon: influence of activated carbon and PFAS characteristics. *Sci. Total Environ.* 795, 148821. <https://doi.org/10.1016/j.scitotenv.2021.148821>.
- Chen, J., Zhang, P. yi, Liu, J., 2007. Photodegradation of perfluorooctanoic acid by 185 nm vacuum ultraviolet light. *J. Environ. Sci.* 19, 387–390. [https://doi.org/10.1016/S1001-0742\(07\)60064-3](https://doi.org/10.1016/S1001-0742(07)60064-3).
- Dang, C., Sun, F., Jiang, H., Huang, T., Liu, W., Chen, X., Ji, H., 2020. Pre-accumulation and in-situ destruction of diclofenac by a photo-regenerable activated carbon fiber supported titanate nanotubes composite material: intermediates, DFT calculation, and ecotoxicity. *J. Hazard Mater.* 400, 123225. <https://doi.org/10.1016/j.jhazmat.2020.123225>.
- Detweiler, Z.M., Wulfsberg, S.M., Frith, M.G., Bocarsly, A.B., Bernasek, S.L., 2016. The oxidation and surface speciation of indium and indium oxides exposed to atmospheric oxidants. *Surf. Sci.* 648, 188–195. <https://doi.org/10.1016/j.susc.2015.10.026>.
- Du, Z., Deng, S., Bei, Y., Huang, Q., Wang, B., Huang, J., Yu, G., 2014. Adsorption behavior and mechanism of perfluorinated compounds on various adsorbents-A review. *J. Hazard Mater.* 274, 443–454. <https://doi.org/10.1016/j.jhazmat.2014.04.038>.
- Gayen, R.N., Hussain, S., Bhar, R., Pal, A.K., 2012. Synthesis and characterization of indium phosphide films prepared by co-evaporation technique. *Vacuum* 86, 1240–1247. <https://doi.org/10.1016/j.vacuum.2011.11.005>.
- Gomez-Ruiz, B., Ribao, P., Diban, N., Rivero, M.J., Ortiz, I., Urriaga, A., 2018. Photocatalytic degradation and mineralization of perfluorooctanoic acid (PFOA) using a composite  $\text{TiO}_2$ -rGO catalyst. *J. Hazard Mater.* 344, 950–957. <https://doi.org/10.1016/j.jhazmat.2017.11.048>.

- Hong, J.Y., Lee, E., Jang, J., 2013. Electro-responsive and dielectric characteristics of graphene sheets decorated with TiO<sub>2</sub> nanorods. *J. Mater. Chem.* 1, 117–121. <https://doi.org/10.1039/c2ta00286h>.
- Huang, D., Yin, L., Niu, J., 2016. Photoinduced hydrodefluorination mechanisms of perfluorooctanoic acid by the SiC/graphene catalyst. *Environ. Sci. Technol.* 50, 5857–5863. <https://doi.org/10.1021/acs.est.6b00652>.
- Jasper, E.E., Ajibola, V.O., Onwuka, J.C., 2020. Nonlinear regression analysis of the sorption of crystal violet and methylene blue from aqueous solutions onto an agro-waste derived activated carbon. *Appl. Water Sci.* 10, 1–11. <https://doi.org/10.1007/s13201-020-01218-y>.
- Javed, H., Metz, J., Eraslan, T.C., Mathieu, J., Wang, B., Wu, G., Tsai, A.L., Wong, M.S., Alvarez, P.J.J., 2020. Discerning the relevance of superoxide in PFOA degradation. *Environ. Sci. Technol. Lett.* 7, 653–658. <https://doi.org/10.1021/acs.estlett.0c00505>.
- Jian, J.M., Chen, D., Han, F.J., Guo, Y., Zeng, L., Lu, X., Wang, F., 2018. A short review on human exposure to and tissue distribution of per- and polyfluoroalkyl substances (PFASs). *Sci. Total Environ.* 636, 1058–1069. <https://doi.org/10.1016/j.scitotenv.2018.04.380>.
- Jiang, F., Zheng, S., An, L., Chen, H., 2012. Effect of calcination temperature on the adsorption and photocatalytic activity of hydrothermally synthesized TiO<sub>2</sub> nanotubes. *Appl. Surf. Sci.* 258, 7188–7194. <https://doi.org/10.1016/j.apsusc.2012.04.032>.
- Kosmulski, M., 2001. Pristine points of zero charge of gallium and indium oxides. *J. Colloid Interface Sci.* 238, 225–227. <https://doi.org/10.1006/jcis.2001.7484>.
- Lawless, D., Serpone, N., Meisel, D., 1991. Role of OH radicals and trapped holes in photocatalysis. A pulse radiolysis study. *J. Phys. Chem.* 95, 5166–5170. <https://doi.org/10.1021/j100166a047>.
- Le, H.A., Linh, L.T., Chin, S., Jung, J., 2012. Photocatalytic degradation of methylene blue by a combination of TiO<sub>2</sub>-anatase and coconut shell activated carbon. *Powder Technol.* 225, 167–175. <https://doi.org/10.1016/j.powtec.2012.04.004>.
- Li, F., Du, P., Liu, W., Li, X., Ji, H., Duan, J., Zhao, D., 2018. Hydrothermal synthesis of graphene grafted titania/titanate nanosheets for photocatalytic degradation of 4-chlorophenol: solar-light-driven photocatalytic activity and computational chemistry analysis. *Chem. Eng. J.* 331, 685–694. <https://doi.org/10.1016/j.cej.2017.09.036>.
- Li, F., Duan, J., Tian, S., Ji, H., Zhu, Y., Wei, Z., Zhao, D., 2020a. Short-chain per- and polyfluoroalkyl substances in aquatic systems: occurrence, impacts and treatment. *Chem. Eng. J.* 380, 122506. <https://doi.org/10.1016/j.cej.2019.122506>.
- Li, F., Wei, Z., He, K., Blaney, L., Cheng, X., Xu, T., Liu, W., Zhao, D., 2020b. A concentrate-and-destroy technique for degradation of perfluorooctanoic acid in water using a new adsorptive photocatalyst. *Water Res.* 185, 1–14. <https://doi.org/10.1016/j.watres.2020.116219>.
- Li, M., Yu, Z., Liu, Q., Sun, L., Nanoparticles, 2016. Photocatalytic decomposition of perfluorooctanoic acid by noble metallic nanoparticles modified TiO<sub>2</sub>. *Chem. Eng. J.* 286, 232–238. <https://doi.org/10.1016/j.cej.2015.10.037>.
- Li, X., Zhang, P., Jin, L., Shao, T., Li, Z., Cao, J., 2012a. Efficient photocatalytic decomposition of perfluorooctanoic acid by indium oxide and its mechanism. *Environ. Sci. Technol.* 46, 5528–5534. <https://doi.org/10.1021/es204279u>.
- Li, Z., Zhang, P., Li, J., Shao, T., Jin, L., 2013a. Synthesis of In<sub>2</sub>O<sub>3</sub>-graphene composites and their photocatalytic performance towards perfluorooctanoic acid decomposition. *J. Photochem. Photobiol. Chem.* 271, 111–116. <https://doi.org/10.1016/j.jphotochem.2013.08.012>.
- Li, Z., Zhang, P., Shao, T., Li, X., 2012b. In<sub>2</sub>O<sub>3</sub> nanoporous nanosphere: a highly efficient photocatalyst for decomposition of perfluorooctanoic acid. *Appl. Catal. B Environ.* 125, 350–357. <https://doi.org/10.1016/j.apcatb.2012.06.017>.
- Li, Z., Zhang, P., Shao, T., Wang, J., Jin, L., Li, X., 2013b. Different nanostructured In<sub>2</sub>O<sub>3</sub> for photocatalytic decomposition of perfluorooctanoic acid (PFOA). *J. Hazard Mater.* 260, 40–46. <https://doi.org/10.1016/j.jhazmat.2013.04.042>.
- Lin, A.W.C., Armstrong, N.R., Kuwana, T., 1977. X-ray Photoelectron/Auger electron spectroscopic studies of tin and indium metal foils and oxides. *Anal. Chem.* 49, 1228–1235. <https://doi.org/10.1021/ac50016a042>.
- Liu, W., Cai, Z., Zhao, X., Wang, T., Li, F., Zhao, D., 2016. High-capacity and photoregenerable composite material for efficient adsorption and degradation of phenanthrene in water. *Environ. Sci. Technol.* 50, 11174–11183. <https://doi.org/10.1021/acs.est.6b02623>.
- Liu, X., Xu, B., Duan, X., Hao, Q., Wei, W., Wang, S., Ni, B.J., 2021. Facile preparation of hydrophilic In<sub>2</sub>O<sub>3</sub> nanospheres and rods with improved performances for photocatalytic degradation of PFOA. *Environ. Sci. Nano* 8, 1010–1018. <https://doi.org/10.1039/d0en01216e>.
- Ma, J., Chen, L., Liu, Y., Xu, T., Ji, H., Duan, J., Sun, F., Liu, W., 2021. Oxygen defective titanate nanotubes induced by iron deposition for enhanced peroxymonosulfate activation and acetaminophen degradation: mechanisms, water chemistry effects, and theoretical calculation. *J. Hazard Mater.* 418, 126180. <https://doi.org/10.1016/j.jhazmat.2021.126180>.
- Minnesota Pollution Control Agency, R. division, 2009. 3M Cottage Grove Site, Proposed Cleanup Plan for PFCs.
- Nguyen, C.K., Low, M.X., Zavabeti, A., Jannat, A., Murdoch, B.J., Della Gaspera, E., Orrell-Trigg, R., Walia, S., Elbourne, A., Truong, V.K., McConville, C.F., Syed, N., Daeneke, T., 2021. Ultrathin oxysulfide semiconductors from liquid metal: a wet chemical approach. *J. Mater. Chem. C* 9, 11815–11826. <https://doi.org/10.1039/d1tc01937f>.
- O'Connell, S.G., Ardent, M., Segars, A., Kimmel, T., Braun-McNeill, J., Avens, L., Schroeder, B., Ngai, L., Kucklick, J.R., Keller, J.M., 2010. Temporal and spatial trends of perfluorinated compounds in juvenile loggerhead sea turtles (*Caretta caretta*) along the east coast of the United States. *Environ. Sci. Technol.* 44, 5202–5209. <https://doi.org/10.1021/es9036447>.
- Ogata, F., Nagai, N., Itami, R., Nakamura, T., Kawasaki, N., 2020. Potential of virgin and calcined wheat bran biomass for the removal of chromium(VI) ion from a synthetic aqueous solution. *J. Environ. Chem. Eng.* 8, 103710. <https://doi.org/10.1016/j.jece.2020.103710>.
- Panchangam, S.C., Lin, A.Y.C., Shaik, K.L., Lin, C.F., 2009. Decomposition of perfluorocarboxylic acids (PFCAs) by heterogeneous photocatalysis in acidic aqueous medium. *Chemosphere* 77, 242–248. <https://doi.org/10.1016/j.chemosphere.2009.07.003>.
- Panchangam, S.C., Yellatur, C.S., Yang, J.S., Loka, S.S., Lin, A.Y.C., Vemula, V., 2018. Facile fabrication of TiO<sub>2</sub>-graphene nanocomposites (TGNs) for the efficient photocatalytic oxidation of perfluorooctanoic acid (PFOA). *J. Environ. Chem. Eng.* 6, 6359–6369. <https://doi.org/10.1016/j.jece.2018.10.003>.
- Park, M., Wu, S., Lopez, I.J., Chang, J.Y., Karanfil, T., Snyder, S.A., 2020. Adsorption of perfluoroalkyl substances (PFAS) in groundwater by granular activated carbons: roles of hydrophobicity of PFAS and carbon characteristics. *Water Res.* 170, 115364. <https://doi.org/10.1016/j.watres.2019.115364>.
- Peng, Y.P., Chen, H., Huang, C.P., 2017. The Synergistic Effect of photoelectrochemical (PEC) reactions exemplified by concurrent perfluorooctanoic acid (PFOA) degradation and hydrogen generation over carbon and nitrogen codoped TiO<sub>2</sub> nanotube arrays (C-N-TNTAs) photoelectrode. *Appl. Catal. B Environ.* 209, 437–446. <https://doi.org/10.1016/j.apcatb.2017.02.084>.
- Qian, L., Georgi, A., Gonzalez-Olmos, R., Kopinke, F.D., 2020. Degradation of perfluorooctanoic acid adsorbed on Fe-zeolites with molecular oxygen as oxidant under UV-A irradiation. *Appl. Catal. B Environ.* 278, 119283. <https://doi.org/10.1016/j.apcatb.2020.119283>.
- Qian, L., Kopinke, F.D., Georgi, A., 2021. Photodegradation of perfluorooctanesulfonic acid on Fe-zeolites in water. *Environ. Sci. Technol.* 55, 614–622. <https://doi.org/10.1021/acs.est.0c04558>.
- Qianqian, Z., Tang, B., Guoxin, H., 2011. High photoactive and visible-light responsive graphene/titanate nanotubes photocatalysts : preparation and characterization. *J. Hazard Mater.* 198, 78–86. <https://doi.org/10.1016/j.jhazmat.2011.10.012>.
- Rahman, M.F., Peldszus, S., Anderson, W.B., 2014. Behaviour and fate of perfluoroalkyl and polyfluoroalkyl substances (PFASs) in drinking water treatment: a review. *Water Res.* 50, 318–340. <https://doi.org/10.1016/j.watres.2013.10.045>.
- Rey, A., Quiñones, D.H., Álvarez, P.M., Beltrán, F.J., Plucinski, P.K., 2012. Simulated solar-light assisted photocatalytic ozonation of metoprolol over titania-coated magnetic activated carbon. *Appl. Catal. B Environ.* 111–112, 246–253. <https://doi.org/10.1016/j.apcatb.2011.10.005>.
- Saeidi, N., Kopinke, F.D., Georgi, A., 2021. What is specific in adsorption of perfluoroalkyl acids on carbon materials? *Chemosphere* 273, 128520. <https://doi.org/10.1016/j.chemosphere.2020.128520>.
- Sawada, Y., Iyanagi, T., Yamazaki, I., 1975. Relation between redox potentials and rate constants in reactions coupled with the system oxygen-superoxide. *Biochemistry* 14, 3761–3764. <https://doi.org/10.1021/bi00688a007>.
- Shao, T., Zhang, P., Jin, L., Li, Z., 2013. Photocatalytic decomposition of perfluorooctanoic acid in pure water and sewage water by nanostructured gallium oxide. *Appl. Catal. B Environ.* 142–143, 654–661. <https://doi.org/10.1016/j.apcatb.2013.05.074>.
- Singh, A.K., 2016. Freundlich adsorption isotherm. In: *Engineered Nanoparticles: Structure, Properties and Mechanisms of Toxicity*. Engineered Nanoparticles, pp. 410–415. <https://doi.org/10.1016/b978-0-12-801406-6.00008-x>.
- Soares, O.S.G.P., Jardim, E.O., Ramos-Fernandez, E.V., Villora-Picó, J.J., Pastor-Blas, M. M., Silvestre-Albergo, J., Orfão, J.J.M., Pereira, M.F.R., Sepúlveda-Escribano, A., 2021. Highly N<sub>2</sub>-selective activated carbon-supported Pt-In catalysts for the reduction of nitrites in water. *Front. Chem.* 9, 1–11. <https://doi.org/10.3389/fchem.2021.733881>.
- Song, Z., Dong, X., Wang, N., Zhu, L., Luo, Z., Fang, J., Xiong, C., 2017. Efficient photocatalytic defluorination of perfluorooctanoic acid over BiOCl nanosheets via a hole direct oxidation mechanism. *Chem. Eng. J.* 317, 925–934. <https://doi.org/10.1016/j.cej.2017.02.126>.
- Tang, H., Xiang, Q., Lei, M., Yan, J., Zhu, L., Zou, J., 2012. Efficient degradation of perfluorooctanoic acid by UV-Fenton process. *Chem. Eng. J.* 184, 156–162. <https://doi.org/10.1016/j.cej.2012.01.020>.
- US EPA, 2022. Drinking water health advisories for PFOA and PFOS [WWW Document]. URL 10.4.21. <https://www.epa.gov/ground-water-and-drinking-water/drinkin-g-water-health-advisories-pfoa-and-pfos>.
- US EPA, 2021a. Basic information on PFAS [WWW Document]. URL 10.4.21. <https://www.epa.gov/pfas/basic-information-pfas>.
- US EPA, 2021b. Per- and polyfluoroalkyl substances (PFAS) [WWW Document]. URL 10.4.21. <https://www.epa.gov/pfas>.
- Vecitis, C.D., Park, H., Cheng, J., Mader, B.T., Hoffmann, M.R., 2009. Treatment technologies for aqueous perfluorooctanesulfonate (PFOS) and perfluorooctanoate (PFOA). *Front. Environ. Sci. Eng. China* 3, 129–151. <https://doi.org/10.1007/s11783-009-0022-7>.
- Wang, J., Chen, B., 2015. Adsorption and coadsorption of organic pollutants and a heavy metal by graphene oxide and reduced graphene materials. *Chem. Eng. J.* 281, 379–388. <https://doi.org/10.1016/j.cej.2015.06.102>.
- Wang, Q., Lei, X., Pan, F., Xia, D., Shang, Y., Sun, W., Liu, W., 2018. A new type of activated carbon fibre supported titanate nanotubes for high-capacity adsorption and degradation of methylene blue. *Colloids Surfaces A Physicochem. Eng. Asp.* 555, 605–614. <https://doi.org/10.1016/j.colsurfa.2018.07.016>.
- Wei, Z., Villamena, F.A., Weavers, L.K., 2017. Kinetics and mechanism of ultrasonic activation of persulfate: an in situ EPR spin trapping study. *Environ. Sci. Technol.* 51, 3410–3417. <https://doi.org/10.1021/acs.est.6b05392>.

- Wei, Z., Xu, T., Zhao, D., 2019. Treatment of per- and polyfluoroalkyl substances in landfill leachate: status, chemistry and prospects. *Environ. Sci. Water Res. Technol.* 5, 1814–1835. <https://doi.org/10.1039/c9ew00645a>.
- Wu, Y., Li, Y., Fang, C., Li, C., 2019. Highly efficient degradation of perfluorooctanoic acid over a MnO<sub>x</sub>-modified oxygen-vacancy-rich In<sub>2</sub>O<sub>3</sub> photocatalyst. *ChemCatChem* 11, 2297–2303. <https://doi.org/10.1002/cctc.201900273>.
- Xu, T., Ji, H., Gu, Y., Tong, T., Xia, Y., Zhang, L., Zhao, D., 2020. Enhanced adsorption and photocatalytic degradation of perfluorooctanoic acid in water using iron (hydr) oxides/carbon sphere composite. *Chem. Eng. J.* 388 <https://doi.org/10.1016/j.cej.2020.124230>.
- Zhu, Y., Xu, T., Zhao, D., Li, F., Liu, W., Wang, B., An, B., 2021. Adsorption and solid-phase photocatalytic degradation of perfluorooctane sulfonate in water using gallium-doped carbon-modified titanate nanotubes. *Chem. Eng. J.* 421, 129676. <https://doi.org/10.1016/j.cej.2021.129676>.